ELSEVIER

Journal of Magnetism and Magnetic Materials 236 (2001) 14–27

Journal of magnetism and magnetic materials

www.elsevier.com/locate/jmmm

Simultaneous structural and magnetic transitions in YFe_4Ge_2 studied by neutron diffraction and magnetic measurements

P. Schobinger-Papamantellos[a,*], J. Rodríguez-Carvajal[b], G. André[b], N.P. Duong[c], K.H.J. Buschow[c], P. Tolédano[d]

[a] *Laboratorium für Kristallographie, ETHZ, CH-8092 Zürich, Switzerland*
[b] *Laboratoire Leon Brillouin, (CEA-CNRS) Saclay, 91191 Gif sur Yvette Cedex, France*
[c] *Van der Waals-Zeeman Institute, University of Amsterdam, NL-1018 XE Amsterdam, The Netherlands*
[d] *Groupe "Structure des Materiaux sous Conditions Extrêmes", SNBL/ESRF, BP 220, 38043 Grenoble Cedex, France*

Received 12 April 2001
Dedicated to the memory of Jean-Pierre Schobinger

Abstract

The magnetic behaviour of the tetragonal YFe_4Ge_2 compound has been studied by neutron diffraction and bulk magnetisation measurements. Magnetic ordering occurs below $T_N = 43.5$ K simultaneously with a structural transition from tetragonal $P4_2/mnm \rightarrow Pnnm$ to orthorhombic symmetry. Both transitions are of first order. The symmetry breaking is connected with primary displacive order parameters involving shifts of the Fe atoms. The Fe site splits into two sites in Pnnm, the shifts of the Fe atoms with respect to the tetragonal phase have opposite signs along the *a* (dilatation) and *b* (contraction) axes. This induces the symmetry breaking tensile strains. The planar canted antiferromagnetic arrangement with eight sublattices is the ground state associated with a magnetic energy involving isotropic exchange and anisotropic (relativistic) interactions. The magnetic structure is invariant under the magnetic space group $P\frac{2_1}{n'}\frac{2_1}{n'}\frac{2_1}{m'}(Sh_{58}^{399})$. The moments of the two orbits have the same value. At 1.5 K the Fe moment equals $0.63(4)\,\mu_B$/Fe atom. The YFe_4Ge_2 magnetostructural phenomena are compared to the more complex analogue of the $ErFe_4Ge_2$ compound. The structural and magnetic transitions are described phenomenologically within a Landau–Dzialoshinski approach which assumes a triggering mechanism, in which the spontaneous strain is triggered by the exchange contribution to the magnetic ordering.

PACS: 75.25+z; 76.30.Kg; 68.35.Rh; 75.80

Keywords: Rare earth germanides; Magnetic structure; Neutron diffraction; Magnetoelastic first order transition

1. Introduction

There exist different classes of magnetostructural effects taking place at magnetic phase transitions. The most commonly studied are the magnetoelectric effect [1] piezomagnetism [2] and magnetostriction. These effects can be predicted

*Corresponding author. Tel.: +41-1-632-37-73; fax: +41-1-632-11-33.
E-mail address: schobinger@kristall.erdw.ethz.ch (P. Schobinger-Papamantellos).

0304-8853/01/$ - see front matter
PII: S0304-8853(01)00442-5

from symmetry considerations showing that the structural modifications are induced by the magnetic ordering, i.e. the structural change represents a secondary mechanism with respect to the primary magnetic mechanism [3]. A less common situation is found when the magnetic and structural transitions arise simultaneously due to a coupling between two primary order-parameters associated with mechanisms of partly different origins. This has been discussed for example in the case of Nickel–iodine boracite [4] in which the ferroelectric, ferroelastic and "latent" antiferromagnetic orders take place at the same critical temperature. However in this latter material it was unclear, due to the intrinsic complexity of the observations, to distinguish which of the primary mechanisms could trigger the others. In the present article we report experimental observations on the magnetostructural transition (ferroelastic and antiferromagnetic) found in the rare earth compound YFe_4Ge_2, in which the coupling between the magnetic and ferroelastic order-parameters can be clearly decomposed, therefore providing an insight into the specific magnetic forces participating to the structural transition.

YFe_4Ge_2, like the heavy rare earth compounds RFe_4Ge_2 where R = Dy, Ho, Er, Lu, was previously reported to crystallise with the $ZrFe_4Ge_2$ type of structure [5] in space group, $P4_2/mnm$. The unit cell is characterised by the lattice constants $a = 7.004$ Å and $c = 3.755$ Å. It contains two formula units with the Zr atoms at 2b: $(0, 0, 1/2)$, the Fe atoms at 8i: $(0.092, 0.346, 0)$ and the Ge atoms at 4g: $(0.2201, -0.2201, 0)$.

The RFe_4Ge_2 compounds were reported to order ferromagnetically with T_C varying between 963 and 643 K for R = Y and Lu, respectively [6]. A later ^{57}Fe Mössbauer study [7] of $DyFe_4Ge_2$ and $ErFe_4Ge_2$ showed no magnetic ordering to be present above about 65 and 44 K, respectively. Recent neutron diffraction and XRPD studies on the magnetic ordering and structure of the $ErFe_4Ge_2$ compound [8] indicated that the magnetic ordering is accompanied by a double structural phase transition. The high temperature (HT) phase disproportionates by a first-order transition into two distinct phases:

$P4_2/mnm\,(T_C,\ T_N = 44\,K) \rightarrow Cmmm$ (majority LT phase) + Pnnm (minority IT Phase) which coexist in proportions varying with temperature down to 4 K. In $ErFe_4Ge_2$ the Cmmm phase is dominating the low temperature (LT) range 1.5–20 K. The highest portion (30%) of the Pnnm minority phase is found in the intermediate temperature (IT) range 20 K–T_N at 30 K. The XRPD data [9] indicated a transition of the Pnnm phase to a monoclinic phase P112/m. The Cmmm phase is associated with a distortion of the tetragonal angle γ, leading to the orthorhombic phase Cmmm with $\boldsymbol{a}_o = \boldsymbol{a}_t - \boldsymbol{b}_t$ and $\boldsymbol{b}_o = \boldsymbol{a}_t + \boldsymbol{b}_t$. The temperature dependent orthorhombic distortion with $a_o/b_o > 1$ could be brought into connection with the onset of the dominant R−R magnetic interaction which is ferromagnetic along a_o and antiferromagnetic along b_o, leading to doubled ($2b_o$) magnetic cell. The Er moment directions are within the plane $(1\,1\,0)_t$ or $(1\,0\,0)_o$. The Pnnm phase is associated with an a_t/b_t1 distortion just below T_N. This phenomenon of a simultaneous occurrence of two-phase transitions most likely originates from the existence of two different competing coupling mechanisms between the R−R and the Fe–Fe magnetic moments and their coupling with lattice strains.

In the present investigation we have focused our attention on YFe_4Ge_2. Because Y is nonmagnetic the magnetic interactions and the concomitant coupling with lattice strains involve only the Fe moments. We will show that here the magnetic transition is accompanied by a single structural $P4_2/mnm \rightarrow$ Pnnm transition. These results lead to a better understanding of the phase transition observed previously in $ErFe_4Ge_2$, which will be discussed.

2. Sample preparation and magnetic measurements

The YFe_4Ge_2 sample used for neutron diffraction was prepared by arc melting of the starting materials of at least 99% purity. Conditions under which YFe_4Ge_2 was the only intermetallic compound present could be only achieved by using an excess of Fe. The sample used in the present experiments has the nominal composition

YFe_5Ge_2. It was wrapped in Ta foil and annealed at 900°C for two weeks in an evacuated quartz tube. After vacuum annealing, the sample was investigated by X-ray diffraction and apart from the main phase of the $ZrFe_4Si_2$ type, it was found to contain about 12% of α-Fe as an impurity phase.

The temperature dependence of the magnetisation was measured in the temperature range 4.2–1200 K. No reliable conclusions could be derived, however, from these data because the magnetic signal of the sample was obscured by the ferromagnetic signal coming from the α-Fe impurity. More revealing are the measurements of the temperature dependence of the ac-susceptibility presented in Fig. 1. Because the magnetization of α-Fe is virtually temperature-independent below 200 K, the α-Fe impurity is not expected to show any discontinuity in the temperature dependence of the AC-susceptibility. The strong peak shown in the low-temperature part of Fig. 1 is therefore attributed to the main phase YFe_4Ge_2, which apparently gives rise to a magnetic phase transition at about 45 K.

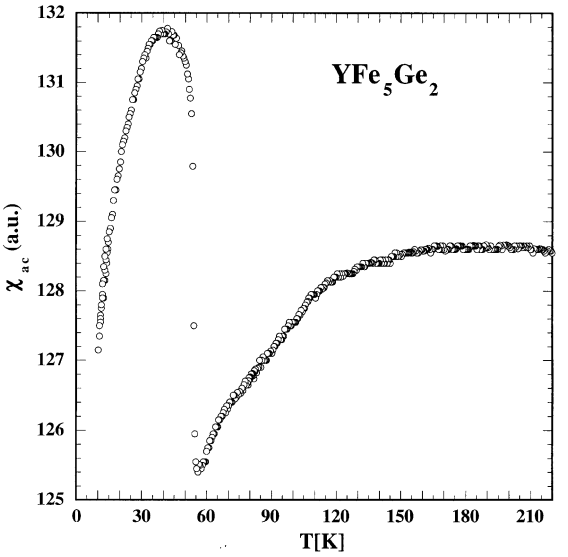

Fig. 1. Temperature dependence of the ac-susceptibility of a sample with nominal composition YFe_5Ge_2.

3. Neutron diffraction

3.1. Data collection and analysis

Neutron diffraction experiments were carried out in the temperature range 1.5–293 K at the facilities of the Orphée reactor (LLB-Saclay) and of the ILL in Grenoble. The LLB-data were collected on the G4.1 (800-cell position sensitive detector, PSD) and G42 (high resolution, HR: 70 detectors with Soller collimators) diffractometers using the wavelengths of 2.426 Å and 2.3433 Å, respectively. The ILL-data were collected with the D1A diffractometer ($\lambda = 1.9114$ Å). The step increment in 2θ was 0.1°. The G4.1 data were collected in the 2θ region 16–96° for a full set of temperatures in the range 1.5–55 K in steps of 3 K in order to study more precisely the magnetic transition and of larger steps (10 K) above it. The HR G42 and D1A data, which extend from 3–160°, were collected for some selected temperatures in the range 1.5–293 K for structural refinements. The data were analysed with the program FullProf [10]. The peak shape was best approximated with a pseudo-Voigt function. Similarly to the $ErFe_4Ge_2$ XRPD refinements [9] a strong anisotropic broadening of Bragg peaks was necessary to be included in the refinements. This broadening is associated with the presence of microstrains induced by the magnetostructural phase transition. The inclusion of strain parameters dropped the R_{wp}-factor from 19% to 10% in the D1A data.

3.2. Crystal structure (HR G42 and D1A data)

The refinements of the HR neutron diffraction patterns collected in the paramagnetic state at 293 K (G42) and 60 K (D1A) (see Fig. 2) led to satisfactory R-factors ($R_B = 2-3\%$, $R_{wp} = 7$–10%) given in Table 1 confirming the tetragonal $ZrFe_4Si_2$ type of structure [5]. The α-Fe reflections in the neutron pattern, denoted by arrows in Fig. 2, were excluded from the refinement.

3.3. First-order ferroelastic transition

The neutron patterns collected below $T_N = 43.5$ K (see Fig. 2) display a completely

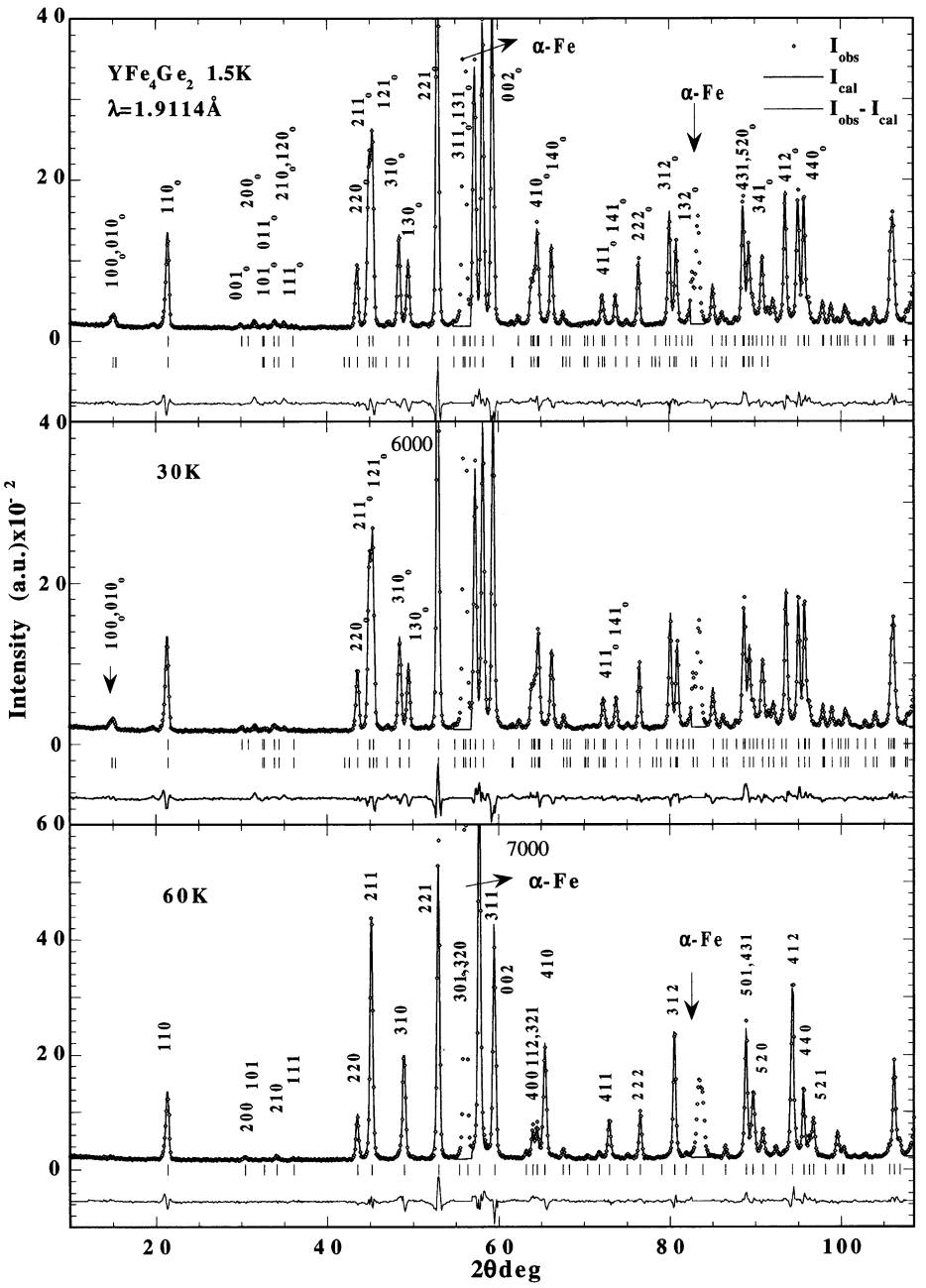

Fig. 2. Observed and calculated neutron intensities of YFe_4Ge_2, in the paramagnetic state at 60 K (bottom) and the magnetically ordered state at 1.5 and 30 K. HR data (D1A diffractometer).

different peak topology than that obtained at 60 K (HR, D1A data). Comparing the 1.5 and 30 K data displayed in Fig. 2 one immediately recognises that all $(h\,h\,l)_t$ tetragonal nuclear reflections remain unchanged while all reflections with hk are split. The splitting becomes more important with increasing $|h-k|$ difference. This fact indicates the breaking of the tetragonal symmetry (as

Table 1
Refined structural parameters of YFe_4Ge_2 from neutron HR data in the paramagnetic state[a]

$P4_2/mnm$	293 K, G42 data			60 K, D1A data	
Atom/site	x	y	z	x	y
Y: 2b	1	0	1/2	0	0
Fe: 8i (x, y, 0)	0.0885(1)	0.3554(2)	0	0.0883(2)	0.35480(2)
Ge: 4g (x, $-x$, 0)	0.2156(1)	−0.2156(1)	0	0.2165(2)	−0.2165(2)
a, b (Å)	0.73148(1)			0.72989(1)	
c (Å), V(Å)^3	0.38671(1)	0.20691(1)		0.38541(1)	0.20533(1)
R_B(%), R_F(%)	2.5, 2.8			3.6, 3.1	
R_{wp}(%), R_{exp}(%)	7.2, 3.5			10.4, 4.3	

[a] The overall temperature factor B_{of} equals 2.0(1) and 1.0(3) Å^2, respectively. R_B, R_F, R_{wp}, R_{exp} are the agreement Bragg-, structure-, weighted profile- and expected- (from the counting statistics) factors.

Table 2
Refined structural parameters of YFe_4Ge_2 from neutron HR data in the magnetically ordered state[a]

Pnnm Atom/site	X	y	z	μ_x (μ_B)	μ_y (μ_B)	μ_T (μ_B)
1.5 K						
Y: 2b	0	0	1/2	—	—	—
Fe1: 4g(x, y, 0)	0.0944(3)	0.3554(5)	0	0.54(5)	−0.34(7)	0.64(2)
Fe2: 4g(x, y, 0)	0.3537(3)	0.0800(2)	0	0.34(7)	−0.54(5)	0.64(2)
Ge: 4g, (x, y, 0)	0.2100(3)	−0.2226(3)	0	—	—	—
a, b (Å), a/b	0.73877(2)	0.72033(6)	1.025			
c (Å), V(Å)3	0.38603(1)	0.20543(3)				
R_B, R_F, R_m(%) = 3.2, 2.3, 23; R_{wp}, R_{exp}(%) = 10, 3.5						
30 K						
Y: 2b	0	0	$\frac{1}{2}$	—	—	—
Fe1: 4g(x, y, 0)	0.0943(3)	0.3555(3)	0	0.54(5)	−0.30(7)	0.62(3)
Fe2: 4g(x, y, 0)	0.3537(3)	0.0834(2)	0	0.30(7)	−0.54(5)	0.62(3)
Ge: 4g, (x, y, 0)	0.2101(2)	−0.2224(3)	0			
a, b (Å), a/b	0.73854(2)	0.72056(1)	1.025			
C (Å), V(Å)3	0.38602(1)	0.20543(1)				
R_B, R_F, R_m(%) = 2.89, 2, 22; R_{wp}, R_{exp}(%) = 9.8, 3.5						

[a] The overall temperature factor was set to $B_{of} = 0.001$ (nm)^2. R_B, R_F, R_m, R_{wp}, R_{exp} as in Table 1.

$(a/b)_t1$) towards orthorhombic. The only orthorhombic subgroup of order 2 of $P4_2/mnm$ that fulfills this condition is Pnnm. The refinement of neutron patterns in the 1.45–45 K range was carried out in the Pnnm space group. Results are summarised in Table 2 for 1.5 and 30 K. The structural parameters and the ratio $a/b = 1.025$ are identical within the 3σ limit.

Fig. 3 shows the jump of the lattice parameters and of the a/b ratio and of the tensile strain $e_1 \approx e_{xx} - e_{yy} = \Delta a/a - \Delta b/b \approx 2|(a-b)/(a+b)|$ at the structural transition found to occur at $T_C = 43.5$ K. The change of about 2×10^{-2} of the tensile strain at the transition clearly denotes the first order character for the ferroelastic change from tetragonal to orthorhombic symmetry [11,12].

The Fe site splits into two 4g orbits while R and Ge reside at the 2b and 4g sites, respectively. The split atomic positions (Fe1 orbit atom: 1–4, Fe1′

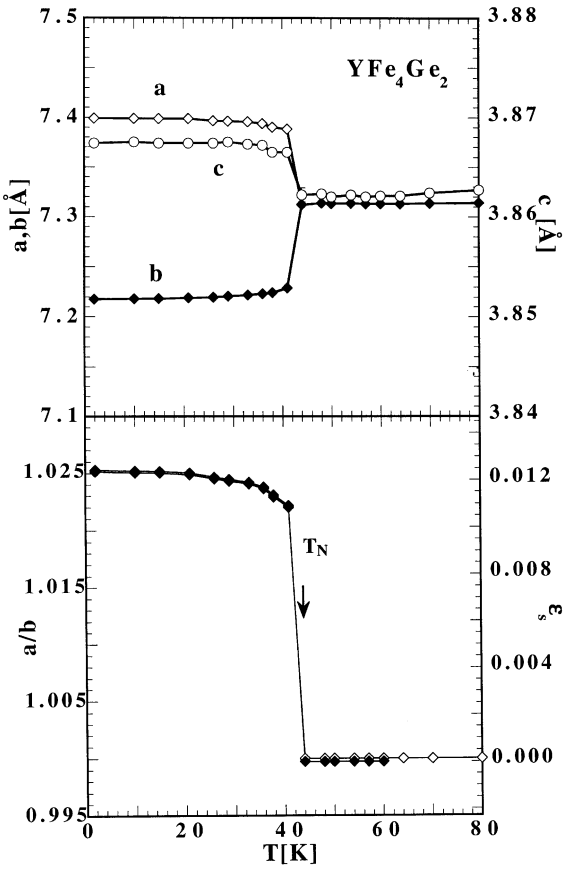

Fig. 3. Temperature dependence of (a) the lattice parameters (top part) (b) of the a/b ratio and the strain parameter $\varepsilon_s 2|(a-b)/(a+b)|e_{xx}-e_{yy}$ of YFe_4Ge_2 (bottom part).

orbit atoms: 1′–4′) and the atomic displacement field for various temperatures above and below the transition are given in Table 3. The Fe atoms related by the m_{xxz} tetragonal mirror operation belong to different orbits. The field of the atomic displacements in Table 3 shows that the major contribution to the macroscopic strain $(e_{xx}-e_{yy})$ responsible for the symmetry lowering is the shifting of the Fe atoms. This is illustrated in Fig. 4 where one can see that the field of displacements of the Fe1 orbit has only $\pm\Delta x$ components whereas the field of the Fe2 orbit has only $\pm\Delta y$ components. These antiparallel displacements along the x and y directions result in a contraction of the b lattice parameter and a dilatation of the a lattice parameter in the orthorhombic cell. The change experienced by the c-axis is reduced by a factor 20 (the c scale is 10 times larger in Fig. 3). The important deformation of the Fe tetrahedron below the transition is shown in the plane (0 0 1) by dotted lines in Fig. 4. On the other hand although the displacements of the Ge atoms are of the same order of magnitude they occur in oblique directions and contribute in a secondary way to the tensile strain $(e_{xx}-e_{yy})$.

The presence of microstrains in all phases treated so far in this work may come from the ferroelastic character of the first order phase transition, at T_C, $T_N \approx 43.5$ K. The coexistence of different domains creates strain fields responsible for the anisotropic broadening of reflections. It is remarkable that the microstrains were found to persist also in the 293 K data, in general it is supposed that above a certain temperature an effective annealing may suppress them. It would be of interest to compare with the strain parameters at 293 K of a sample not previously cooled down to 1.5 K.

3.4. The magnetic transition

The patterns obtained at 1.5 and 30 K comprise a fairly important intensity contribution to the forbidden nuclear (100/010) reflections located at 18.5°. This fact suggests the existence of antiferromagnetic order with the same cell size as the nuclear one, $\mathbf{q}=0$. There are six magnetic space groups associated with the Pnnm space group and $\mathbf{q}=0$ [13,14]. These are given on the top part of Table 4 together with the magnetic modes of the general 8h and of the 4g Fe sites. For collinear structures with four sublattices the modes are defined [15]

$$\begin{aligned}\vec{m} &= \vec{\mu}_1+\vec{\mu}_2+\vec{\mu}_3+\vec{\mu}_4,\\ \vec{\ell}_1 &= \vec{\mu}_1-\vec{\mu}_2+\vec{\mu}_3-\vec{\mu}_4,\\ \vec{\ell}_2 &= \vec{\mu}_1+\vec{\mu}_2-\vec{\mu}_3-\vec{\mu}_4,\\ \vec{\ell}_3 &= \vec{\mu}_1-\vec{\mu}_2-\vec{\mu}_3+\vec{\mu}_4.\end{aligned} \quad (1)$$

For an orthorhombic structure with eight sublattices one has the eight vectors

$$\begin{aligned}&\vec{L}_{iu}=\vec{\ell}_{iu}+\vec{\ell}'_{iu}, \quad \vec{L}^{-}_{iu}=\vec{\ell}_{iu}-\vec{\ell}'_{iu},\\ &\vec{M}_u=\vec{m}_u+\vec{m}'_u, \quad \vec{M}^{-}_u=\vec{m}_u-\vec{m}'_u,\end{aligned} \quad (2)$$

Table 3
Splitting of the YFe_4Ge_2 atomic positions for the structural ($P4_2/mnm \rightarrow Pnnm$) transition occuring at $T_N >= 43.5\,K$. Δx, Δy are the atomic displacements and $\Delta x/x = e_{xx}$, $\Delta y/y = e_{yy}$ are the strain components between $T = 60\,K > T_N >$ and $T = 30\,K < T_N >$

		$P4_2/mnm$					Pnnm			Δx	Δy
		x	y	z			x	y	z	$\Delta x/x$	$\Delta y/y$
Y: 2b	1	0	0	1/2	Y1: 2b	1	0	0	1/2	0	0
	2	1/2	1/2	0		2	1/2	1/2		0	0
Fe: 8i	1	x	y	0	Fe1: 4g	1	x	y	0	+0.006	+0.0007
										0.068	0.0019
	2	$-x$	$-y$	1/2		2	$-x$	$-y$	1/2	−0.006	−0.0007
										0.068	0.0019
	3	$-y+1/2$	$x+1/2$	1/2		3	$-x+1/2$	$Y+1/2$	1/2	−0.006	+0.0007
										0.068	0.0019
	4	$y+1/2$	$-x+1/2$	1/2		4	$x+1/2$	$-y+1/2$	1/2	+0.006	−0.0007
										0.068	0.0019
	5	$-x+1/2$	$y+1/2$	1/2		1′	y	x	0	−0.0011	−0.0049
										0.003	0.055
	6	$x+1/2$	$-y+1/2$	1/2		2′	$-y$	$-x$	0	+0.0011	−0.0049
										0.003	0.055
	7	y	x	0		3′	$-y+1/2$	$x+1/2$	1/2	+0.0011	−0.0049
										0.003	0.055
	8	$-y$	$-x$	0		4′	$Y+1/2$	$-x+1/2$	1/2	−0.0011	+0.0049
										0.003	0.055
Ge: 4g	2	x	$-x$	0	Ge: 4g	1	x	y	0	−0.006	−0.0059
										0.0292	0.027
	2	$-x$	x	0		2	$-x$	$-y$	0	+0.006	+0.0059
										0.0292	0.027
	2	$-x$	x	0		2	$-x$	$-y$	0	+0.006	+0.0059
										0.0292	0.027
	3	$-x+1/2$	$-x+1/2$	1/2		3	$-x+1/2$	$-y+1/2$	1/2	+0.006	+0.0059
										0.0292	0.027
	4	$-x+1/2$	$x+1/2$	1/2		4	$x+1/2$	$y+1/2$	1/2	−0.006	+0.0059
										0.0292	0.027

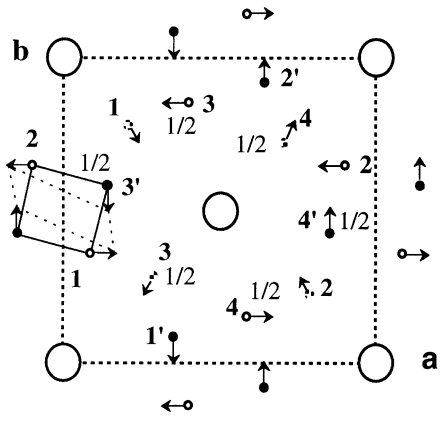

where $\vec{\ell}'_{i\alpha}, \vec{m}'_{\alpha}$ the modes for the last four atoms, $i = 1, 3, u = (xyz)$ Because the Fe atoms are located in an m_z plane, their ordering is restricted to either m_x and/or m_y components or to an m_z component. The best-refined model comprises the modes (ℓ_{3x}, ℓ_{1y}) and (ℓ'_{3x}, ℓ'_{1y}) for the two orbits of type 4g and correlated moment values.

These modes are invariant under the $P^{2_1}_{n'}{}^{2_1}_{n'}{}^{2_1}_{m'}$ (Sh^{399}_{58}) magnetic space group. The refined Fe moment value does not exceed $0.63(4)\,\mu_B$/atom

Fig. 4. Projection of the displacive $P4_2/mnm \rightarrow Pnnm$ mechanism in the plane (0 0 1). The arrows indicate the displacement field. The displacement field of the two Fe orbits has either $\pm\Delta x$ (orbit 1: atoms 1–4) or $\pm\Delta y$ (orbit 2 atoms: 1′–4′). The labeling of the atoms is from Tables 3 and 4.

Table 4
Magnetic space groups and modes associated with the Pnnm space group and the wave vector $\mathbf{q}=0$, for the general position 8h and the special Fe 4g position at the mirror plane m_z[a]

No. 8h	Gen. el.	$P\frac{2_1}{n}\frac{2_1}{n}\frac{2}{m}$			$P\frac{2_1}{n}\frac{2_1}{n}\frac{2}{m}$			$P\frac{2_1}{n'}\frac{2'_1}{n}\frac{2'}{m}(Sh_{58}^{395})$			$P\frac{2'_1}{n}\frac{2'_1}{n}\frac{2'}{m'}(Sh_{58}^{396})$			$P\frac{2'_1}{n'}\frac{2'_1}{n'}\frac{2}{m}(Sh_{58}^{397})$			$P\frac{2_1}{n}\frac{2'_1}{n'}\frac{2'}{m'}(Sh_{58}^{398})$			$P\frac{2_1}{n'}\frac{2_1}{n'}\frac{2}{m'}(Sh_{58}^{399})$		
					L_{3x}	L_{1y}	L_{2z}	M_x^-	L_{2y}^-	L_{1z}^-	L_{3x}^-	L_{3y}^-	M_z^-	L_{1x}	L_{3y}	M_z	M_x	L_{2y}	L_{1z}	L_{3x}^-	L_{1y}^-	L_{2z}^-
1	E	x	y	z	$+u$	$+v$	$+w$	$+u$	$+v$	$+w$	$+u$	$+v$	$+w$	$+u$	$+v$	$+w$	$+u$	$+v$	$+w$	$+u$	$+v$	$+w$
2	2_z	$-x$	$-y$	z	$-$	$-$	$+$	$+$	$+$	$-$	$-$	$-$	$+$	$-$	$-$	$+$	$+$	$+$	$-$	$-$	$-$	$+$
3	2_{1y}	$1/2-x$	$1/2+y$	$1/2-z$	$-$	$+$	$-$	$+$	$-$	$+$	$+$	$-$	$+$	$+$	$-$	$+$	$+$	$-$	$+$	$-$	$+$	$-$
4	2_{1x}	$1/2+x$	$1/2-y$	$1/2-z$	$+$	$-$	$-$	$+$	$-$	$-$	$-$	$+$	$+$	$-$	$+$	$+$	$+$	$-$	-	$+$	$-$	$-$
5	I	$-x$	$-y$	$-z$	$+$	$+$	$+$	$-$	$-$	$-$	$-$	$-$	$-$	$+$	$+$	$+$	$+$	$+$	$+$	-	$-$	$-$
6	M_z	x	y	$-z$	$-$	$-$	$+$	$-$	$-$	$+$	$+$	$+$	$-$	$-$	-	$+$	$+$	$+$	$-$	$+$	$+$	$-$
7	N_y	$1/2+x$	$1/2-y$	$1/2+z$	$-$	$+$	$-$	$-$	$+$	$-$	$-$	$+$	$-$	$+$	-	$+$	$+$	$-$	$+$	$+$	$-$	$+$
8	n_x	$1/2-x$	$1/2+y$	$1/2+z$	$+$	$-$	$-$	$-$	$+$	$+$	$+$	$-$	$-$	$-$	$+$	$+$	$+$	$-$	$-$	$-$	$+$	$+$
4g							ℓ_{2z}			ℓ_{1z}	ℓ_{1x}	ℓ_{3y}				m_z	m_x	ℓ_{2y}		ℓ_{3x}	ℓ_{1y}	
1	e	x	y	0			$+$			$+$	$+$	$+$				$+$	$+$	$+$		$+$	$+$	
2	2_z	$-x$	$-y$	0			$+$			$-$	$-$	$-$				$+$	$+$	$+$		$-$	$-$	
3	2_{1y}	$1/2-x$	$1/2+y$	1/2			$-$			$+$	$+$	$-$				$+$	$+$	$-$		$-$	$+$	
4	2_{1x}	$1/2+x$	$1/2-y$	1/2			$-$			$-$	$-$	$+$				$+$	$+$	$-$		$+$	-	

[a] The symbols used for the axial vectors representing "collinear" magnetic structures for four sublattices are from [15]. For the 8h positions the symbols are defined $\vec{L}_{iu}=\rightarrow\ell_{iu}+\rightarrow\ell'_{iu}, \vec{L}^-_{iu}=\rightarrow\ell_{iu}-\rightarrow\ell'_{iu}, \vec{M}_u=\vec{m}_u+\vec{m}'_u, \vec{M}^-_u=\vec{m}_u-\vec{m}'_u, \rightarrow\ell'_{iu}, \vec{m}'_u$ are the modes for the last four atoms, $i=1,3$, $u=(xyz)$ see also Section 3.2.

Table 5
Irreducible representations (IR) of the $P4_2/mnm1$ space group for $\mathbf{k}=0$. The IC of the paramagnetic space group$P4_2/mnm1'$ are straightforwardly derived[a]

IR	Dim τ_I	$n_i x$ dim(τ_I)	Fe1	Fe2	Fe3	Fe4	Fe5	Fe6	Fe7	Fe8	Labels of basis functions
τ_1	1	1	$(0\,0\,w)$	$(0\,0\,w)$	$(0\,0\,\bar{w})$	$(0\,0\,\bar{w})$	$(0\,0\,\bar{w})$	$(0\,0\,\bar{w})$	$(0\,0\,w)$	$(0\,0\,w)$	$L^-_{2z}=\ell_{2z}-\ell'_{2z}$
τ_2	1	1	$(0\,0\,w)$	$(0\,0\,w)$	$(0\,0\,w)$	$(0\,0\,w)$	$(0\,0\,w)$	$(0\,0\,w)$	$(0\,0\,w)$	$(0\,0\,w)$	$M_z=m_z+m'_z$
τ_3	1	1	$(0\,0\,w)$	$(0\,0\,w)$	$(0\,0\,\bar{w})$	$(0\,0\,\bar{w})$	$(0\,0\,w)$	$(0\,0\,w)$	$(0\,0\,\bar{w})$	$(0\,0\,\bar{w})$	$L_{2z}=\ell_{2z}+\ell'_{2z}$
τ_4	1	1	$(0\,0\,w)$	$(0\,0\,w)$	$(0\,0\,w)$	$(0\,0\,w)$	$(0\,0\,\bar{w})$	$(0\,0\,\bar{w})$	$(0\,0\,\bar{w})$	$(0\,0\,\bar{w})$	$M^-_z=m_z-m'_z$
τ_5	2	8	$(u+p,v+q,0)$	$(u+p,v+q,0)$	$(u-p,v-q,0)$	$(u-p,v-q,0)$	$(u'+p',v'+q',0)$	$(u'+p',v'+q',0)$	$(u'-p',v'-q',0)$	$(u'-p',v'-q',0)$	$m_x;m_y;m'_x;m'_y;$ $\ell_{2x};\ell'_{2x};\ell_{2y};\ell'_{2y}$
τ_6	1	2	$(u\,v\,0)$	$(\bar{u}\,\bar{v}\,0)$	$(\bar{u}\,v\,0)$	$(u\,\bar{v}\,0)$	$(v\,u\,0)$	$(\bar{v}\,\bar{u}\,0)$	$(\bar{v}\,u\,0)$	$(v\,\bar{u}\,0)$	$\ell_{3x}+\ell'_{1y};\ell_{1y}+\ell'_{3x}$
τ_7	1	2	$(u\,v\,0)$	$(\bar{u}\,\bar{v}\,0)$	$(u\,\bar{v}\,0)$	$(\bar{u}\,v\,0)$	$(\bar{v}\,\bar{u}\,0)$	$(v\,u\,0)$	$(\bar{v}\,u\,0)$	$(v\,\bar{u}\,0)$	$\ell_{1x}-\ell'_{3y};\ell'_{3y}-\ell'_{1x}$
τ_8	1	2	$(u\,v\,0)$	$(\bar{u}\,\bar{v}\,0)$	$(\bar{u}\,v\,0)$	$(u\,\bar{v}\,0)$	$(\bar{v}\,\bar{u}\,0)$	$(v\,u\,0)$	$(v\,\bar{u}\,0)$	$(\bar{v}\,u\,0)$	$l_{3x}-l'_{1y};l_{1y}-l'_{3x}$
τ_9	1	2	$(u\,v\,0)$	$(\bar{u}\,\bar{v}\,0)$	$(u\,\bar{v}\,0)$	$(\bar{u}\,v\,0)$	$(v\,u\,0)$	$(\bar{v}\,\bar{u}\,0)$	$(v\,\bar{u}\,0)$	$(\bar{v}\,u\,0)$	$\ell_{1x}+\ell'_{3y};\ell'_{3y}+\ell'_{1x}$
τ_{10}	2	4	$(0\,0\,w+p)$	$(0\,0\,\bar{w}+\bar{p})$	$(0\,0\,\bar{w}+\bar{p})$	$(0\,0\,w'+p')$	$(0\,0\,\bar{w}'+\bar{p}')$	$(0\,0\,\bar{w}'+\bar{p}')$	$(0\,0\,\bar{w}'+\bar{p}')$	$(0\,0\,\bar{w}'+\bar{p}')$	$\ell_{1z};\ell'_{1z};\ell_{3z};\ell'_{3z}$

[a] We give the notation used by Zak et al. [16] and we use the notation given in text to label the basis functions. The atomic components of the basis functions for site 8i are also given. The decomposition of the reducible representation induce by the Fe atoms in 8i for axial vectors is: $\Gamma=\tau_1\oplus\tau_2\oplus\tau_3\oplus\tau_4\oplus4\tau_5\oplus2\tau_6\oplus2\tau_7\oplus2\tau_8\oplus2\tau_9\oplus2\tau_{10}(\Gamma=\sum_{\oplus}n_i\tau_i)$ The coefficients n_i indicate the number of times the IR τ_i is contained in G. The number of independent basis functions for the IR$\tau_i n_i x$ dim (τ_i). This is also the number of free parameters of the magnetic structure.

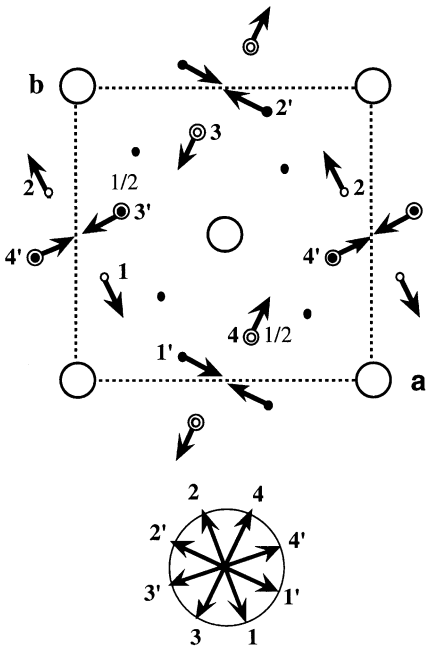

Fig. 5. Schematic representation of the YFe_4Ge_2 magnetic structure of YFe_4Ge_2 at 1.5 K when viewed along [0 0 1]. The labels 1–4 and 1′–4′ denote the atoms of the Fe1 and Fe2 orbits, respectively. The lower part displays the orientations of the eight sublattices.

at 1.45 K and remains almost unchanged at 30 K (0.61(3) μ_B/atom). The moments at the two Fe positions have the same magnitude but are coupled in such a way that their in-plane components almost restore the symmetry of the lost tetragonal 4_2 axis. As can be seen in Fig. 5, Fe1 at (0.094, 0.355, 0) of orbit I has the moment components (0.54(6), −0.32(7), 0) μ_B and Fe1′ at (0.354, 0.08, 0) of orbit II has the moment components (0.32(7), −0.54(6), 0) μ_B. Neglecting the changes of the refined (x, y, 0) parameters of the Fe1 and Fe1′ sublattices the 4_2 symmetry operation would lead to the following transformations: Fe1 → Fe3′ → Fe2 → Fe4′ → Fe1. The corresponding moment rotation angle is ϕ, $270+\phi$, $180+\phi$, $90+\phi$, ϕ, which corresponds to the rotation properties of a left screw or a $4_2'$ axis. The total structure can be described as a planar canted antiferromagnetic structure with 8 sublattices (1–4 and 1′–4′) as shown in the lower part of Fig. 5. This structure corresponds exactly to the basis functions of the

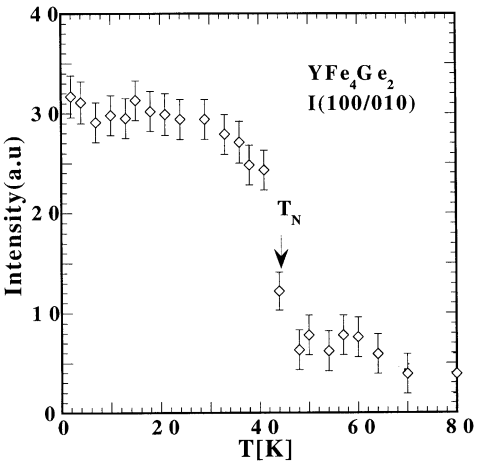

Fig. 6. Thermal variation of the magnetic reflection (100/010) indicating the onset of magnetic order at $T_N = 43.5$ K.

irreducible representation τ_8 of the tetragonal space group $P4_2/mnm$ for the site 8i (see Table 5).

Fig. 6 shows the thermal variation of the integrated magnetic intensity of the strongest resolved magnetic reflection (100/010) (G4.1 data). The figure reflects (a) that the magnetic transition has also a *first order character* with an abrupt intensity change at $T_N = 43.5$ K and (b) that the antiferromagnetic ordering takes place at the *same temperature* as the structural transition. The non-zero intensity value above T_N is attributed to a small magnetic contribution of a partly overlapping impurity phase, which disappears above 70 K.

4. Phenomenological description of the structural and magnetic transitions

In this section we successively describe the symmetry and thermodynamic features characterising the structural (Section 4.1) and the magnetic (Section 4.2) changes which occur below $T_C = T_N = 43.5$ K in YFe_4Ge_2. In Section 4.3 the nature of the simultaneity of the corresponding transition mechanism is discussed.

4.1. Structural phase-diagram of RFe_4Ge_2 (R = Y, Er)

A theoretical approach to the $P4_2/mnm \rightarrow Pnnm$ ferroelastic transition in YFe_4Ge_2 has to be

inserted within a general description of the more complete phase diagram involving the $P4_2/mnm \rightarrow Cmmm$ and $Pnnm \rightarrow P2/m$ transitions recently reported in $ErFe_4Ge_2$ [9]. As shown in Ref. [11] the $P4_2/mnm \rightarrow Pnnm$ symmetry change corresponds to the onset of the spontaneous tensile strain $e_1 \approx e_{xx} - e_{yy}$, which transforms as the one-dimensional irreducible representation (IR) denoted τ_3 of the $P4_2/mnm$ space group. Analogously the $P4_2/mnm \rightarrow Cmmm$ ferroelastic transition gives rise to the spontaneous shear strain $e_2 \approx e_{xy}$ coinciding with another one-dimensional IR of the $P4_2/mnm$ group, denoted by τ_4 in [11]. Therefore, the Landau expansion associated with the reducible representation $\tau_3 + \tau_4$ can be written:

$$F(T, e_1, e_2) = F_0(T) + a_1 e_1^2 + a_2 e_1^4 + a_3 e_1^6 + \cdots b_1 e_1^2 + b_2 e_1^4 + b_3 e_1^6 \cdots + \delta e_1^2 e_2^2, \quad (3)$$

where the a_i, b_i phenomenological coefficients are combinations of second (a_1, b_1) and higher-order ($a_2, a_3, b_2, b_3 \ldots$) elastic constants [11] e.g., $a_1 = c_{11} - c_{12}$, $a_2 = c_{1111} - 4c_{1112} + 3c_{1122}$, $b_1 = c_{66}$, $b_2 = c_{666}$ etc, δ is a coupling coefficient.

In order to obtain a possible first-order transition regime between the parent $P4_2/mnm$ structures and the Pnnm and Cmmm structures, one needs to expand F up to at least the sixth degree terms in e_1 and e_2 and to biquadratic δ-coupling. Minimisation of F with respect to e_1 and e_2 yields *four* possible stable states, which are represented in the theoretical phase diagram of Fig. 7:

I. The parent tetragonal phase which is stable for $a_1 \geqslant 0, b_1 \geqslant$.

II. The orthorhombic Pnnm phase corresponding to the equilibrium strains

$$e_1^e = [\frac{-a_2 + (a_2^2 - 3a_1a_3)^{1/2}}{3a_3}]^{1/2} \quad (4)$$

and

$$e_2^e = 0.$$

III. The orthorhombic Cmmm phase corresponding to

$$e_2^e = 0[\frac{-b_2 + (b_2^2 - 3b_1b_3)^{1/2}}{3b_3}]^{1/2} \quad (5)$$

and

$$e_1^e = 0.$$

IV. A monoclinic phase of symmetry P2/m associated with the equilibrium values $e_1^e \neq 0$ and $e_2^e \neq 0$ where e_1^e and e_1^e are given by the equations of state

$$a_1 + 2a_2(e_1^e)^2 + 3a_3(e_1^e)^4 + \delta(e_2^e)^2 = 0, \quad (6)$$

$$b_1 + 2b_2(e_2^e)^2 + 3b_3(e_2^e)^4 + \delta(e_1^e)^2 = 0. \quad (7)$$

The P2/m space group is the maximal subgroup common to Pnnm and Cmmm, i.e. this phase can be reached from the orthorhombic phases either across a first-order transition or through a second-order transition, the two regimes being separated by tricritical points denoted T_{C_1} and T_{C_2} in Fig. 7. The thermodynamic path followed in our experiment on YFe_4Ge_2 is represented by a straight arrow in Fig. 7, whereas for $ErFe_4Ge_2$ (Ref. [9]) it follows the more complex path shown by a curved arrow, i.e. it crosses the region of coexistence of two orthorhombic phases, between the limit stability lines denoted 2–3 and 3–2 in Fig. 7, on the side where the Cmmm phase is in majority, before going to the Pnnm side where it crosses the $Pnnm \rightarrow P2/m$ transition line.

4.2. The magnetic transition in YFe_4Ge_2

Let us analyse theoretically the paramagnetic-antiferromagnetic transition $P4_2/mnm1' \rightarrow Pn'n'm'$ reported in Section 3.4 for $YFe_4G_{e_2}$. We use here the notations for collinear structures described in 3.4. To construct the different magnetic modes characterising a magnetic structure with eight sublattices associated with the two orbits μ_i and μ_i' $(i = 1 - 4)$ (see Figs. 4 and 5) forming the antiferromagnetic structure in a tetragonal space group one cannot strictly use the same labeling of the basis functions of the irreducible representations used for the orthorhombic position 8h in Table 4 due to the mixture of (xy) components. The transformation properties of the vectors

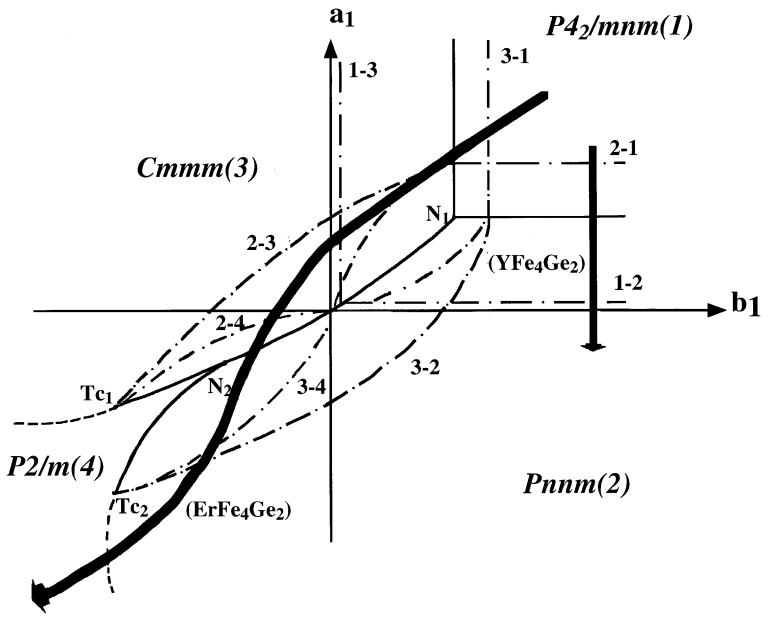

Fig. 7. Phase diagram corresponding to the minimisation of the free-energy F given by Eq. (1) for $a_2<0, b_2<0, \delta>0, a_2^2-3a_1a_3$ and $b_2^2-3b_1b_2>0$. Solid lines are first-order transition lines. Dotted lines are second-order transition lines. Dashed-dotted lines are limit of stability lines of the four phases (1–4 are defined in the figure). The limits of stability lines are labeled in the following way. The line 3–2 denotes the stability of phase 3 in phase 2, and the line 2–3 the stability of phase 2 in phase 3. The straight and curved arrows indicate, respectively, the thermodynamic paths presumably followed in our experiment on YFe_4Ge_2 and $ErFe_4Ge_2$.

$\vec{M}$, $\vec{M}^{-}$, $\vec{L}_i$, $\vec{L}_i^{-}$, $\vec{m}$, $\vec{m}'$, $\vec{\ell}_i$, $\vec{\ell}'_i$ and their components with respect to the irreducible representations of $P4_2/mnm1'$ for the Fe 8i position in YFe_4Ge_2 are summarised in Table 5. One can verify the following:

(1) The magnetic modes $\ell_{3x}-\ell'_{1y}$ and $\ell_{1y}-\ell'_{3x}$ have been found to transform as the antiferromagnetic structure of YFe_4Ge_2 below T_N. These modes correspond to the basis of the same one-dimensional IC, denoted τ_8 in Zak's notation [16]. These modes determine the relativistic contribution (F_m^{rel}), which counts for the anisotropic exchange to the magnetic Landau expansion F_m

$$\begin{aligned}F_m^{rel} &= \tfrac{a_1}{2}(\ell_{3x}-\ell'_{1y})^2+\tfrac{b_1}{4}(\ell_{3x}-\ell'_{1y})^4\\ &+\tfrac{a'_1}{2}(\ell_{1y}-\ell'_{3x})^2+\tfrac{b'_1}{4}(\ell_{1y}-\ell'_{3x})^4\\ &+c(\ell_{3x}-\ell'_{1y})(\ell_{1y}-\ell'_{3x})\\ &+d(\ell_{3x}-\ell'_{1y})^2(\ell_{1y}-\ell'_{3x})^2. \qquad (8)\end{aligned}$$

(2) The isotropic exchange forces give rise to an exchange Hamiltonian that is invariant with respect to an arbitrary rotation in the spin space [15]. The phase transition to a magnetically ordered state driven by exclusive isotropic exchange interactions takes place via a single IR of the group of the Hamiltonian which has a higher symmetry than the magnetic space group. It can be demonstrated that each IR of the space group generates an IR of the exchange group. The basis functions of the permutational representation for 8 atoms and axial vectors are vectors of 8-components (+1 or –1) corresponding to the 8 vectors describing collinear magnetic structures ($\vec{M}$, $\vec{M}^{-}$, $\vec{L}_i$, $\vec{L}_i^{-}$ ($i=1, 2, 3$)).If we consider the particular case of the basis functions $\ell_{3x}-\ell'_{1y}$ and $\ell_{1y}-\ell'_{3x}$, they involve the antiferromagnetic vectors ($\vec{\ell}_1$, $\vec{\ell}_3$) which span a two-dimensional IC denoted τ_{10} [16], and provide the form of the exchange contribution (F_m^{rel}) to F_m:

$$\begin{aligned}&F_m^{ex}(\vec{\ell}_1,\vec{\ell}_3)\\ &\quad=\tfrac{a}{2}(\ell_1^2+\ell_3^2)+\tfrac{b_1}{4}(\ell_1^2+\ell_3^2)^2+\tfrac{b_2}{2}\ell_1^2\ell_3^2. \qquad (9)\end{aligned}$$

Minimising the total expansion $F_m = F_0(T) + F_m^{ex} + F_m^{rel}$ with respect to the relevant variables would lead to tetragonal antiferromagnetic structures, and to obtain the orthorhombic antiferromagnetic structure reported for YFe_4Ge_2 one has also to take into account the structural modification occurring at $T_C = T_N$. This can be made by considering the magnetoelastic coupling to the strain components (e_1, e_2), which have been shown to arise below T_C. The magnetoelastic free energy F_{me} can again be split into its exchange (F_{me}^{ex})and relativistic (F_{me}^{rel}) parts, which are

$$F_{me}^{ex}(\ell_1, \ell_3, e_1, e_2) = \lambda_1(\ell_1^2 - \ell_3^2)e_1 + \lambda_2\ell_1^2\ell_3^2 e_2, \tag{10}$$

$$\begin{aligned} F_{me}^{rel}&(\ell_{3x} - \ell'_{1y}, \ell_{1y} - \ell'_{3x}, e_1, e_2) \\ &= e_1^2[\lambda_3(\ell_{3x} - \ell'_{1y})^2 + \lambda_4(\ell_{1y} - \ell'_{3x})^2] \\ &\quad + e_2^2[\lambda_5(\ell_{3x} - \ell'_{1y})^2 + \lambda_6(\ell_{1y} - \ell'_{3x})^2] \\ &\quad + (\ell_{3x} - \ell'_{1y})(\ell_{1y} - \ell'_{3x})(\lambda_7 e_1^2 + \lambda_8 e_2^2). \end{aligned} \tag{11}$$

Note in Eq. (11) the biquadratic character of the couplings between the (ℓ_{iu}, ℓ'_{iu}) and strain components which results from the property that the magnetic and strain components transform as distinct one-dimensional IC's of the paramagnetic structure. Note also that the primed components would lead to the same coupling invariants and have not been explicitly expressed. In addition one has to add the spontaneous elastic energy truncated at the lowest degree

$$F_{el}(e_1, e_2) = a_1 e_1^2 + b_1 e_2^2. \tag{12}$$

Because of its biquadratic form the relativistic magnetoelastic contribution F_{me}^{rel} does not induce any spontaneous strain below $T_N = T_C$. In contrast, the exchange magnetoelastic contribution F_{me}^{rel} yields the equilibrium-induced strains

$$(e_1^e)_{ex} = -\frac{\lambda_1}{2a_1}(\ell_1^2 - \ell_3^2), \tag{13}$$

$$(e_2^e)_{ex} = -\frac{\lambda_2}{2b_1}\ell_1^2\ell_3^2. \tag{14}$$

Introducing these expressions in F^{ex} and minimising F^{ex} with respect to (ℓ_1 and ℓ_3) leads to four possibles antiferromagnetic exchange orderings: I. $\ell_1 \neq 0$ and $\ell_3 = 0$, II. $\ell_1 = 0$ and $\ell_3 \neq 0$, III, IV: $\ell_1 = \pm\ell_3 \neq 0$. As in the Pn′n′m′ antiferromagnetic structure found in YFe_4Ge_2 one has $e_1^e \neq 0$ and $e_2^e \neq 0$, only the two first solutions I and II have to be considered, since solutions III and IV would lead to $e_2^e \neq 0$. It is straightforward to show that solutions I and II are equivalent and coincide with the moment distribution shown in Fig. 5. One actually finds for the solutions I and II the equilibrium moduli:

$$\begin{aligned} &I.\quad \vec{\ell}_1^{\,e} = \left[\frac{-\alpha}{\beta_1 + \dfrac{\lambda_1^2}{a_1}}\right]^{1/2}, \quad |\vec{\ell}_3^{\,e}| = 0, \\ &II.\quad \vec{\ell}_3^{\,e} = \left[\frac{-\alpha}{\beta_1 + \dfrac{\lambda_1^2}{a_1}}\right]^{1/2}, \quad |\vec{\ell}_1^{\,e}| = 0. \end{aligned} \tag{15}$$

Although the spontaneous strain which takes place at $T_C = T_N$ has a purely exchange origin, coinciding with the onset of the exchange (ℓ_1 and ℓ_3) magnetic modes, the magnetic ordering has both an exchange and relativistic origin. The relativistic contribution, which is responsible of the canting of the sublattices, can be obtained by a minimisation of F_m^{rel} with respect to $\ell_{3x} - \ell'_{1y}$ and $\ell_{1y} - \ell'_{3x}$. One finds the equations of state

$$\begin{aligned} &(\ell_{3x} - \ell'_{1y})[a_1 + b_1(\ell_{3x} - \ell'_{1y})^2] \\ &\quad + c(\ell_{1y} - \ell'_{3x}) + d(\ell_{1y} - \ell'_{3x})^2 = 0, \end{aligned} \tag{16}$$

$$\begin{aligned} &(\ell_{1y} - \ell'_{3x})[a'_1 + b'_1(\ell_{1y} - \ell'_{3x})^2] \\ &\quad + c(\ell_{3x} - \ell'_{1y}) + d(\ell_{3x} - \ell'_{1y})^2 = 0, \end{aligned} \tag{17}$$

which give rise: (1) to a stable state I corresponding to the trivial solution $\ell_{3x} = \ell'_{1y}$ observed in our experiment $\ell_{1y} = \ell'_{3x}$ which preserves the constraints of the high symmetry tetragonal space group and (2) to a state II with $\ell_{3x} \neq \ell'_{1y}$ and $\ell_{1y} \neq \ell'_{3x}$ that correspond to pure orthorhombic phases. Fig. 8 shows the phase diagram in which the two states are inserted. It displays a second-order transition line between the states I and II, and an isostructural (first-order) transition line between two variants of phase II. These two variants coexist at a critical point K of the liquid-gas type, which is not observed in our experiment.

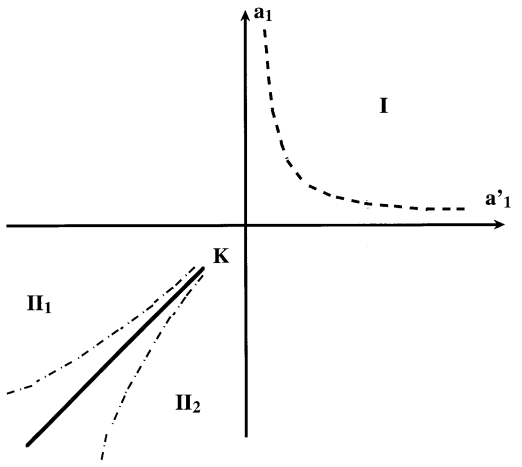

Fig. 8. Phase diagram corresponding to the equations of state (16) and (17), in the plane (a_1, a_1'). Dashed, full and dotted lines are second-order, first-order and limit of stability lines respectively. K is a critical point of the liquid-gas type.

4.3. Nature of the simultaneous structural and magnetic transitions

The property of the spontaneous strain e_1^e, as expressed by Eq. (13), to be induced by a magnetic order-parameter is currently adopted for the description of magnetostructural transitions [12]. It derives from the form of the magnetoelastic coupling terms (Eq. (10) that are linear in the structural quantities (e_1, e_2) and quadratic in the magnetic exchange modes ($\vec{\ell}_i$), due to the additional invariance of the structural quantities by the time-reversal symmetry. Generally however, the magnetic and structural transitions occur at distinct critical temperatures as for example in the class of magnetic materials in which the Jahn-Teller effect plays an important role, e.g. in $KCuF_3$, $LaMnO_3$ or Mn_3O_4. On the other hand, magnetic transitions generally involve a small magnetostrictive effect, which does not give rise to a noticeable spontaneous strain. In YFe_4Ge_2 the simultaneity of the two transitions $T_C = T_N$ can be understood in the framework of the triggering mechanism described by Holakovsky [17] in which the "primary" magnetic order-parameter (ℓ_1, ℓ_3) triggers the "secondary" strain e_1, the two quantities arising at the same temperature due to the jump of the order-parameter components at the first-order transition. The magnitude of the spontaneous strain can be explained by the exchange nature of the triggering magnetic order-parameter, which is large, compared with the numbers usually found when relativistic forces are involved. There exists, to our knowledge, at least one other example of simultaneous magnetic and structural transitions induced by exchange forces, which is $Ni_3B_7O_{13}I$ (Ref. [12], p. 341).

At the microscopic level, it has been stressed in Section 3.3 that the structural change is essentially due to the displacements of the iron ions, which also contribute to the antiferromagnetic order. In this respect, since Eq. (10) actually expresses the coupling between two mechanisms which are both symmetry-breaking and may take place independently but are coupled due to the first order character of the transition (which favours the triggering mechanism), it is meaningless to speculate which of the corresponding order-parameters (displacements or antiferromagnetic order) triggers the other.

5. Concluding remarks

YFe_4Ge_2 like the other isomorphic RFe_4Ge_2 compounds (R = Dy, Ho, Er, with $T_N < 70$ K) orders antiferromagnetically. The magnetic ordering at $T_N = 43.5$ K is accompanied by a first-order phase transition from tetragonal symmetry ($P4_2/mnm$) to orthorhombic symmetry (Pnnm). Presumably the symmetry breaking is related to two primary order parameters (i) the displacement field of the same atom (Fe) (ii) the antiferromagnetic order of the same atoms with in-plane spin components. It has been also shown that only exchange forces take part in the structural ordering, whereas exchange and relativistic forces are both involved in the magnetic order. As the Y ion is non-magnetic the magnetostructural coupling is restricted to the Fe atoms. The low-temperature crystal structure observed in YFe_4Ge_2 is identical to that of a similar phase observed in $ErFe_4Ge_2$. In the latter compound this structure coexists in variable amounts (not exceeding 30%) only in the IT range (20–35 K) with the Cmmm orthorhombic

phase. Most likely the $P4_2/mnm \Rightarrow Pnnm$ phase transition is driven in both compounds by Fe–Fe interactions. The shortest interatomic Fe–Fe distances are those within the compact tetrahedron (see Table 6). If the dominant Fe–Fe interaction would be purely antiferromagnetic, this arrangement would have probably led to a frustrated possibly non-magnetic state [18,19] as reported for spinel and pyrochlores and the Laves phases YMn_2 and $ScMn_2$. However, most of the compounds with tetrahedral arrangements order at lower temperatures by secondary mechanisms.

In the case of YFe_4Ge_2 the planar antiferromagnetic canted structure realised at low temperatures indicates firstly the existence of a considerable anisotropy within the basal plane, and secondly that the Fe–Fe interactions are not exclusively antiferromagnetic. The magnetic ordering of the minority $ErFe_4Ge_2$ Pnnm phase has not yet been elucidated. For this reason a detailed microscopic model that would take into account semiquantitavely the respective influence of the Er and the Fe ions in order to distinguish which of the two types of interactions dominates is not yet feasible. Furthermore in a previous investigation [9] we found that the $P4_2/mnm \Rightarrow Pnnm$ transition in $ErFe_4Ge_2$ is suppressed at lower temperatures by the increasing importance of the R–R and R–Fe interactions which promote the $P4_2/mnm \Rightarrow Cmmm$ transition. Further studies on related RFe_4Ge_2 compounds are planned in the near future in order to better understand this interesting interplay between crystal and magnetic structures and the features that have been foreseen at the phenomenological level.

Table 6
Fe–Fe interatomic distances in (Å) in the compact Fe tetrahedra for various temperatures[a]

Distance	Pnnm		$P4_2/mnm$
	1.5 K	30 K	60 K
Fe1–Fe3′	2.563(1)	2.563(2)	2.606(1)
Fe1–Fe4′	2.660(2)	2.659(2)	2.606(1)
Fe1–Fe2	2.506(3)	2.505(3)	2.481(2)
Fe4′–Fe3′	2.472(3)	2.471(3)	2.481(2)

[a] The labeling of the Fe atoms corresponds to that of Figs. 4 and 5.

In summary, we have described a magnetostructural transition, which displays a number of uncommon features. In particular the simultaneity of the structural and magnetic orders which both correspond to symmetry breaking order-parameters, is due to a triggering mechanism in which the magnetic forces induce the displacements associated with the ferroelastic deformation. Besides, the form of the coupling between the mechanisms allows to clearly determine which type of magnetic interaction is involved in the magnetostructural effect.

References

[1] I.E. Dzialoshinskii, Sov. Phys. JETP 10 (1957) 628.
[2] I.E. Dzialoshinskii, Sov. Phys. JETP 6 (1957) 621.
[3] P. Tolédano, Ferroelectrics 161 (1994) 257.
[4] P. Tolédano, H. Schmid, M. Clin, J.P. Rivera, Phys. Rev. B 32 (1985) 6006.
[5] Ya.P. Yarmoluk, L.A. Lysenko, E.I. Gladyshevski, Dopov. Akad. Nauk Ukr. RSR, Ser. A 37 (1975) 279.
[6] O.Ya. Oleksyn, Yu.K. Gorelenko, O.I. Bodak, in: 10th International Conference on Solid Compounds of Transition Elements, Münster, May 21–25, 1991, P-254-FR, SA.
[7] A.M. Mulders, P.C.M. Gubbens, Q.A. Li, F.R. de Boer, K.H.J. Buschow, J. Alloys Compounds 221 (1995) 197.
[8] P. Schobinger-Papamantellos, J. Rodríguez-Carvajal, G. André, C.H. de Groot, F.R. de Boer, K.H.J. Buschow, J. Magn. Magn. Mater. 191 (1999) 261.
[9] P. Schobinger-Papamantellos, J. Rodríguez-Carvajal, K.H.J. Buschow, J.E. Dooryhee, A.N. Fitch, J. Magn. Magn. Mater. 210 (2000) 121.
[10] J. Rodríguez-Carvajal, Physica B 192 (1993) 55. The manual of FullProf can be obtained at: http://www-llb.cea.fr/fullweb/powder.htm.
[11] P. Tolédano, M.M. Fejer, B.A. Auld, Phys. Rev. B 27 (9) (1983) 5717.
[12] J.C. Tolédano, P. Tolédano, The Landau Theory of Phase Transitions, World Scientific, Singapore, 1987.
[13] V.A. Koptzik, Shubnikov Groups, Moscow University print, Moscow, 1966.
[14] W. Opechowski, R. Guccione, in: G.T. Rado, H. Suhl (Eds.), Magnetism IIA, Academic Press, London, 1965, p. 105 (Chapter 3).
[15] I.E. Dzialoshinskii, Sov. Phys. JETP 5 (1957) 1259.
[16] J. Zak, A. Casher, M. Glück, Y. Gur, The Irreducible Representations of Space Groups, Benjamin, New York, 1969.
[17] J. Holakovsky, Phys. Status Solidi B 56 (1973) 615.
[18] M.J. Harris, S.T. Bramwell, T. Zeiske, D.F. McMorrow, P.J.C. King, J. Magn. Magn. Mater. 177–181 (1998) 757.
[19] M. Shiga, K. Fujisawa, H. Wada, J. Phys. Soc. Jpn. 62 (1993) 1329.